Study on the Influencing Factors of Spontaneous Wettability Transition Behaviour on Metallic-based Surfaces

Jie Wang[a,b], Mengjuan Wu[c] and Xianghui Hou[c]*

[a] School of Materials Science and Engineering, Nanjing Institute of Technology, Nanjing 211167, China;

[b] Jiangsu Key Laboratory of Advanced Structural Materials and Application Technology, Nanjing 211167, China;

[c] Faculty of Engineering, University of Nottingham, University Park, Nottingham NG7 2RD, UK;

*Correspondence: xianghui.hou@nottingham.ac.uk;

Abstract: Hydrophobic surfaces and coatings have attracted more and more interest in recent years due to their broad applications in diverse areas. In many cases, a metallic surface would demonstrate a reversible wettability from hydrophilic state to hydrophobic state spontaneously. However, the wetting behavior and hydrophobic mechanism of metallic surfaces are far from clear. In this work, 304 stainless steel (SS) surface and Ni-Cu-P coatings have been chosen to investigate the intrinsic mechanism of the surface wettability transition with the help of X-ray photoelectron spectroscopy (XPS) and ambient air/vacuum storage treatment. The surface topographies, wetting behaviors and surface chemistry were studied systemically. The results showed that the water contact angle (WCA) variation of the as-prepared surfaces changing from hydrophilic state to hydrophobic state is largely associated with the surface specific area. The recovery of water repellency is related to a time constant which mainly depends on the micro-scale surface convolution or surface roughness. Rougher surface tends to accelerate the surface adsorption of airborne hydrocarbon species in the ambient atmosphere, leading to a more intensive WCA increase. The study

provides a generic theoretical justification for relevant time-dependent wettability studies.

Keywords: Wettability; WCA recovery; Surface roughness; Surface adsorption

1. Introduction

Due to the broad technological potentials, hydrophobic surfaces and coatings find extensive applications in diverse modern industrial areas, including self-cleaning, anti-icing, non-sticking, corrosion resistance and so forth [1-4]. Undoubtedly, it is always of scientific and practical importance to pay more attention to the R&D of the hydrophobic coatings.

However, during the study of the hydrophobic metallic surfaces, an unusual feature of spontaneously changing wettability phenomenon has been discovered and the time-dependent wettability has been confirmed [5, 6]. For example, Liu et al reported that a smooth metallic Au surfaces could become hydrophobic merely by introducing micro/nanostructures without any additional surface modification [7]. Zhu et al prepared sputtered Cu films with micro-square holes exhibiting transitional wettability from hydrophilic to hydrophobic [8].

By figuring out the underlying mechanisms of wettability transition, a controllable surface wettability could be fairly alluring, which has wide application prospects, e.g., in controlled transportation of fluids, tunable wettability devices and so on. For surfaces with good wettability, it could help to control the reagent flow in a

microfluidic channel [9].

Researchers are making strides to understand the rate and extent of the WCA recovery processes. For example, Zhang et al studied the changing wettability on sputtered Cu films with micro-scale patterns and further investigated the role of roughening effect of micro-structures on the wetting transition [8]. Florian et al reported that the wetting behavior on an alloy steel could be tuned by inducing controlled surface morphology change with the implemented laser structuring strategies [10].

There are arguments on the wettability transition process of metallic surfaces [11-13]. One explanation is that the recovered hydrophobicity could be plagued by the adsorption of nonpolar contaminants such as carbon species to the surface [14]. Or it could be the function of a short-range reorganization and the surface substances may have reorientation and present a lower energy surface [15]. It is of particular importance for the preparation and engineering applications for hydrophobic coatings. The analysis on the spontaneous wettability transition of the surfaces regarding the effect of airborne hydrocarbon groups need to be most attempted. There are diverse methods that can be used to modify the surfaces, including UV/ozone treatment [16], and plasma treatment [17]. The plasma treatment could be one of the relatively fast, simple and cost-effective methods for surface modification [18]. No chemical solvents and poisonous gases will be used during the process, and it is a simple approach to tailor the surface state using plasma treatment without alerting the bulk properties [19].

In this work, the reversible wettability phenomenon and the influencing factors that affect such a transition with different metallic surfaces were studied. The details of spontaneous wettability transition of stainless steel (SS) samples and Ni-Cu-P coatings with different surface morphologies had been analyzed. By investigating the changes of WCA after the plasma cleaning and the subsequent storage in ambient air, it was found that higher surface specific area would prompt more airborne hydrocarbon species adsorbed onto the surface. A rough surface, which means a high surface specific area, could accelerate the surface adsorption of airborne hydrocarbon species in the ambient atmosphere. This work would help to build a critical understanding of the wettability transition and surface chemistry towards the reversible wettability of metallic surfaces.

2. Experimental

2.1 Materials

304 stainless steel plates were used as the substrates and the research objects. Nickel foil (Shenzhen Changsheng Telecom Technology Co. Ltd, China, 99.96%) was applied as the anode of electrodeposition. Nickel sulfate hexahydrate ($NiSO_4 \cdot 6H_2O$), copper sulfate pentahydrate ($CuSO_4 \cdot 5H_2O$) and sodium dihydrogen phosphate (NaH_2PO_2) from Sigma-Aldrich (Dorset, UK) were used as the starting chemicals of nickel, copper and phosphorus, respectively. Other agents including sodium citrate dihydrate ($C_6H_5Na_3O_7 \cdot 2H_2O$), ammonium chloride ($NH_4Cl$), succinic acid, hydrochloric acid (HCl), sodium acetate, sodium molybdate (Na_2MoO_4), tin chloride

($SnCl_2$), palladium chloride ($PdCl_2$), citric acid ($C_6H_8O_7$), sodium dodecyl sulfate (SDS) and sodium sulfate (Na_2SO_4) were also acquired from Sigma-Aldrich. All of the chemicals were analytical grade reagents and used as received. Deionised water with a resistivity of 18.2 MΩ•cm was used in the process of coating preparation.

2.2 Coating fabrication

The 304 SS substrates were cut into rectangular pieces with a dimension of 50mm×20mm×1mm. First, for the SS surface study, several SS samples with different surface roughness were prepared. The as-received SS substrates were designated as SS-AR. The samples that were ground by 240 p, 400 p, 800 p and 1200 p grit abrasive papers and then polished by 6 μm and 1 μm diamond paste were designated as SS-polish. And the samples that underwent a sandblasting treatment (Guyson Formula 1200 cabinet using F220 with alumina, average size 68 μm) were named SS-rough.

Then the Ni-Cu-P coatings were prepared using electrodeposition and electroless deposition methods, respectively. To ensure the comparability of the electrodeposited samples and electroless deposited samples, the substrates were also sandblasted prior to the coating deposition. The electrodeposited coatings and electroless-deposited coatings were both prepared with the methods reported in our previous work [20, 21]. The electrodeposited coatings and electroless-deposited coatings were also selected as the research objects and designated as ED and ELD, respectively.

After these samples were prepared, an aging process was conducted. The as-prepared samples were stored indoor in ambient air condition for certain durations as

the aging treatment. The relative humidity was monitored at around 45 ± 10%, and the ambient temperature was 20 ± 3°C. Besides, an aging study of ED and ELD samples was also conducted in vacuum bags for certain periods. To quickly remove the adsorbed substances on the coating surface, plasma cleaning was carried out for a duration of 8 min using a Plasma Cleaner (Model 1020, Fischione) with a gas mixture of 25 vol% oxygen and 75 vol% argon. The vacuum degree of the plasma cleaner (the ultimate vacuum could reach 1×10^{-7} mbar) during the plasma cleaning was around 60-100 Pa [22].

2.3 Microstructural characterisation

Surface morphologies of the samples were characterised by a JEOL-6490LV SEM equipped with an energy-dispersive X-ray spectroscopy (EDX, INCA, Oxford Instrument Link ISIS-3000) under an acceleration voltage of 20 kV. 3D topography of the coating surfaces was acquired using a non-contact optical profiler (Zeta-20, KLA-Tencor). The surface compositions and binding energy of the involved elements were characterised by an X-ray photoelectron spectroscopy (XPS) (Kratos AXIS ULTRA LiPPS, Kratos Analytical Limited) with a mono-chromated Al kα X-ray source (1486.6 eV) operated at 10 mA emission current and 12 kV anode potential (120 W). The electron emission angle for the photoelectron analyser was 90°. The size of the analytical area was 300μm×700μm. No sputter-etching process was performed on the coating samples. The analysis chamber pressure was controlled to be lower than 5×10^{-9} mbar which could be achieved by the cooperative work of turbomolecular and ion

pumps. A low-energy electron charge neutralizer was used in all measurements to prevent sample charging during the operation [23, 24]. Then the obtained results were further analysed using CasaXPS software.

2.4 Evaluation of wettability

The wettability of the samples was characterised using a contact angle goniometer (FTA200, First Ten Angstroms, Inc., Portsmouth, VA, USA) with a pumping out rate of 1 μL/s and a fixed droplet volume of 5 μL at room temperature and humidity condition. For every sampling at controlled time point, a minimum of five measurements had been performed.

3. Results

3.1 Wettability transition on different sample surfaces

WCA evolution curves of the 304 SS substrates with different surface roughness before and after plasma cleaning are shown in Fig.1. The stabilized WCAs of the three samples were 90.6±1.5° for SS-polish, 99.9±2.8° for SS-AR and 126.8±2.9° for SS-rough, respectively. Their initial stabilized WCAs were different which mainly come from the variations of the surface roughness. After the plasma cleaning, these samples were stored in ambient air for aging, and the wettability was also monitored. The plasma treatment results in a remarkable change to the wettability of all the studied samples. A sharp decrease in WCA takes place after the plasma cleaning and

then the WCAs gradually increase with the aging in ambient air.

For SS-polish, it took around 1 day exposure in air for the WCA to rise from 19.1±0.6° to 81.6±3.6°. It was then saturated at around 85° after further aging. There was no drastic change in WCA for the next 3 days (maintained at level of around 85°). Similarly for SS-AR, the WCA increased from 17.5±1.2° and the value is finally stabilized at around 100° after one day aging without any obvious change for the next 3 days (maintained at level of around 100°). The SS-rough demonstrated a much larger variation in WCA decrease and increase among the studied SS samples. The WCA decreased from 126.8±2.9° to only 10.8±0.1° after the plasma cleaning. With the subsequent aging in ambient air, the WCA showed a quite steady increase, and it took around 40 hours for the surface to restore its hydrophobicity. The WCA kept increasing to the previous level after 2 days, prior to the saturation.

For the ED and ELD samples, as shown in Fig.1(d) and Fig.1(e), similar changing trends are observed. The ELD sample first suffered a sharp decrease from 106.1±4.2° to 17.7±0.9°. After that, with aging in air, the measured WCA rose and nearly recovered to its former level after around 32 h. The spontaneous change in surface wettability of the ED coating was quite similar to that of the ELD coating. The surface became hydrophilic after the plasma cleaning, showing a WCA of 7.8±0.2°. Then the WCA increased slowly and the sample took around 55 h to become hydrophobic again. The WCA gradually recovered to its former value (nearly 140°) after around 7 days aging. With further air exposure, its WCA remained at that level. It suggested that all these sample surfaces sensitively responded to the plasma

cleaning, while the levels of the WCA recovery varied.

3.2 Effect of airborne hydrocarbons and reversible wettability transition

The ED samples and ELD samples had also been selected to investigate the reversibility of the wettability transition. Once the ED and ELD samples were prepared, their initial WCAs were measured immediately. The WCA measurements were conducted every 24 h (including the values just after the plasma cleaning) to verify the temporal variation of the surface wettability. Similar WCA variations could be obtained from Fig.1(d) and Fig.1(e). The initial WCAs of the as-prepared ED and ELD samples were 9.8±0.1° and 17.2±0.2°, respectively (shown as "Measurement 1" in Fig.2). Then the two samples were stored in ambient air for 7 days. The WCAs of ED and ELD rose to 140.8±4.6° and 103.8±2.8° after the whole air exposure, which was marked as "Measurement 2". Then an 8 min plasma cleaning was performed. The WCAs of both samples decreased sharply, lower than 20° (marked as "Measurement 3"). The wettability showed dramatic transition from hydrophilic to hydrophobic and back to hydrophilic. The ED and ELD were put back into the ambient atmosphere again to repeat such a transition cycle. To extensively evaluate the reversible wettability, several cycles had been conducted on ED and ELD samples. Again, both samples demonstrated the repeatable transition from hydrophilic to hydrophobic. The multi-transition of the WCAs indicated good reversibility of the wettability.

To better crosscheck the effects of airborne hydrocarbons and minimise the influences from the individual features between the ED and ELD samples, both

samples were put into vacuum bags and stored for the comparison purposes. It is easy to find that the WCAs of ED and ELD samples remain unchanged after the same durations of storage in vacuum. Whereafter, both samples were taken out and transferred into air again, and the transition of wetting behaviors (from hydrophilic to hydrophobic) clearly occurred (marked as "Measurement 8").

3.3 Surface morphology and surface roughness of the studied surfaces

Surface morphology of different samples are characterised and shown in Fig.3. 3D topography images indicating the surface roughness are also provided here. For SS-polish, no visible features could be observed at the scale of the performed SEM images. The surface roughness (Ra) is only 0.06±0.01 μm after the polishing. Then for the as-received substrates, SS-AR, no further treatment has been carried out. The SS-AR sample is generally flat with only a few surface features and no visible inclusions on the surface. The 3D topography image shows that the measured Ra is 0.2±0.01 μm, reflecting a very smooth and flat surface. For SS-rough, the sandblasting treatment has been conducted. The surface becomes much rougher, exhibiting regular hierarchical structures, consisting of various surface scratches and striations. The measured Ra is 1.0±0.03 μm.

In Fig.4, it could be observed that the surface of the ED sample consists of some large scale regular features (Fig.4(a)), including cauli-flower like structures and nodule structures. The surface of ED sample shows the feature of dual-scale roughness, similar to the surface of lotus leaf. The size of the cauli-flower-like

structures is around a few microns, and the measured Ra could reach 3.9±0.1 μm. For the ELD samples (Fig.4(c)), it exhibits a less hierarchical morphology compared with the ED sample. No obvious crack and void could be observed. A kind of shallow nodular structures with the size around a few microns could be observed. The measured Ra of the ELD sample is 0.5±0.02 μm.

EDX analysis was conducted on ED and ELD samples before and after the plasma cleaning treatment to monitor the changes of the surface chemical compositions. Hydrogen cannot be characterized here. It is found that the EDX results nearly remain unchanged during the plasma cleaning and ambient atmosphere storage, the atomic ratios of C and O of ED stabilized at around 23% for C and 5.6% for O, respectively. While for ELD sample, the atomic ratios of C and O maintained at around 20% for C and 1.8% for O, as shown in Tab.S1 in Supplementary Materials.

3.4 XPS analysis of samples versus different treatments

Fig.5 shows high resolution XPS spectra of the ED samples before and after plasma cleaning. The survey spectrum of the ED samples is also provided in Fig.S1 for reference. All of the data including the measured raw data, resolved component peaks and the fitted lines have been demonstrated in the figures based on the authoritative data presentation manner [25]. Fig.5 shows the main changes of the C 1s and O 1s peaks, respectively. First, the C 1s spectra of the ED coatings could be decomposed into several Gaussian-Lorentzian peaks according to proposed nomenclatures [26]. During the spectra alignment, it is noted that the binding energy

(BE) scale of C 1s peaks (including C-C/C-H bonds) of the airborne hydrocarbon (adventitious carbon) referenced may not be reliable [27, 28]. Currently, the widely used BE value range for C 1s peak is normally 284.6-285.2eV, which is arbitrary chosen and suggested by the ISO standard [29]. This has not been justified yet and it may lead to unphysical results, like a non-zero density of states above the Fermi level [30]. Greczynski et al suggested that if the specified sample possesses density of states at the Fermi level, the density-of-states (DOS) close to the Fermi level could be measured and the Fermi edge could then be used as the energy reference [31]. Besides, Greczynski et al also suggested another method: for independent material systems, E_B^F of C 1s peak is closely related to the sample work function (indicating that the electronic levels of the adventitious carbon layer align to the vacuum level), which could be acquired by ultraviolet photoelectron spectroscopy (UPS) in the same instrument [32]. Considering the studied ED and ELD samples in this work, they all have decent electrical conductivity, the referenced binding energy scale for C 1s could be set at 289.58 - Φ_{SA} eV. The reason is that there is weak interaction between the adsorbed adventitious carbon layer and the underlying sample, the vacuum-level alignment implies that a complementary measurement of Φ_{SA} allows the use of the C 1s peak for the purpose of binding-energy scale calibration [32]. In this study, as the binding energy of the adventitious C1s peak is not constant, literature values of the work function of Ni-Cu-P coating were used to minimize the error. For Ni-Cu-P coatings (ED and ELD samples), as reported by Dorgelo, the work function of alloy films range between the values of the individual pure metals [33]. Besides, the

phosphorus in ED and ELD samples are both in amorphous state, no Ni related or Cu related compound could be detected from the XRD analysis, the main phase is NiCu for ED and $Cu_{0.81}Ni_{0.19}$ (as indicated in Supplementary Material Fig.S4). So the work function of Ni-Cu alloys is the main consideration here, and the work function for Ni-Cu-P coating has been estimated mainly by Ni-Cu alloy [34]. Cheng et al reported that the concentration of Cu atoms had little effect on the work function [35], and the calculated work functions for Ni-Cu alloys with 0 % and 30 % contents are both 4.91 eV, which is also consistent with that of MoTa alloys [36]. From Tab.S1, the difference in Cu contents between ED (Cu: around 6%) and ELD (Cu: around 5%) samples did not bring much difference to the work function, so 4.91 eV has been set as the work function of ED and ELD samples. The BE of C 1s peaks is calculated to be 284.67 eV. Besides, the peaks were not used for the binding energy reference for evaluating the detailed positions of the resolved carbon groups. Only the specific ratios of different resolved carbon groups were calculated and discussed. Apart from this, to minimize the error, the Ar 2p3/2 peak that locates at 241.82 eV has also been used to guide the amount by which core-level peaks are shifted from the neutral positions for the aim to confirm with the calibration of the binding energy scale [37, 38]. It enables that all of the core detected levels could be aligned accordingly “by hand” when all of the XPS spectra are finished. Under this situation, the C 1s spectrum was resolved with four photoelectron peaks, which consist of C=C, C-C/C-H, C-O/C-O-C and COOH/C=O. The fittings of the peaks are mainly conducted based on the constraint of the intensity ratio between each peak. The peaks C=C and C-C/C-

H are classified as the hydrocarbon groups, which take the predominate role. The overall ratio of hydrocarbon shows an obvious decrease from 87.1% to 72.1%. The O 1s peak of the ED coatings also could be decomposed into several constituent satellite peaks based on the nomenclature proposed by Khan [39]: O-metal groups, C-OH/C-O and O-H-O, including lattice oxygen (mainly O-metal groups) and non-lattice oxygen (corresponding to C-OH/C-O and O-H-O). The relative atomic ratio of the lattice oxygen is 21.9% and 36.6% before and after plasma cleaning, respectively. In particular, the plasma cleaning treatment could largely increase the number of the surface lattice oxygen groups. The detailed results of the atomic ratios of the hydrocarbon and lattice oxygen groups have been listed in Tab.1.

Fig.6 shows high resolution XPS spectra of the ELD samples during the long storage in ambient air and after plasma cleaning. The methodology applied for the decomposition of the C 1s and O 1s peaks could be the same as the one used before. Referring to the constraint of the intensity ratio of the involved groups, the fitting process has also been carried out. During the storage, it is clear that the overall atomic ratio of the airborne hydrocarbon groups (C=C and C-C/C-H) increase from 74.0% to 81.7%, as shown in Tab.1. By taking the WCA variation during the ambient air storage into consideration, the above groups are the major compositions of the adsorbed hydrocarbon. While for O 1s, the O-metal group shows a clear decreasing trend, from 50.6% to 15.1%. Conversely, the relative contents of the non-lattice oxygen groups (O-H-O and C-OH/C-O) increase dramatically from 49.4% to 84.9%. The WCA increase in Fig.6 could be ascribed to the decrease of the lattice oxygen

groups.

Apart from the C 1s and O 1s spectra, other detected core signals including Ni 2p and Cu 2p have also been analyzed and shown in Supplementary Material Fig.S2 and Fig.S3. In Fig.S2, the Ni 2p spectrum could be resolved with four photoelectron peaks, which consist of Ni 2p3/2, Satellite 3/2, Ni 2p1/2 and Satellite 1/2, the main peaks are assigned to nickel ions with divalent oxidation state, while the satellite peak is normally to confirm the existence of divalent nickel because of the multiple splitting in the energy levels of the transition metals [40]. While for Cu 2p, the Cu 2p 3/2 and Cu 2p 1/2 peaks have been decomposed into several constituent satellite peaks including Cu/Cu^{+}, Cu^{2+}, Satellite 3/2 and Satellite 1/2, which can be assigned to Cu/Cu_2O and CuO species, respectively [7]. Besides, the atomic ratios of different component peaks are also listed in Supplementary Material Tab.S2 and Tab.S3. It is observed that the atomic ratio of Ni 2p related groups nearly remains unchanged after the plasma cleaning, indicating little variation has taken place during the plasma cleaning treatment. For Cu 2p, as indicated in Tab. S3, the atomic ratios of the relative groups also show little change versus the plasma cleaning. Not only the Cu/Cu^{+} groups that are resolved from both Cu 2p3/2 and Cu 2p1/2 peaks, but also Cu^{2+}, satellite 3/2 and satellite 1/2 peaks all remain at the same level. The plasma cleaning did not introduce much changes to the Ni 2p and Cu 2p groups.

4. Discussion

From the wettability study, it shows that the WCA value is a function of the

surface roughness. The samples with larger surface roughness exhibit sharper WCA decrease and lower WCA values after the plasma cleaning. According to the Wenzel model, the apparent contact angle (θ_w) on a homogeneous rough surface could be expressed as Eq (1) [41]:

$$\cos\theta_w = r(\cos\theta) \quad (1)$$

Where r refers to the roughness ratio, showing the ratio between the real area of the solid surface and its projection area. θ is the contact angle of the sample surface. It is easy to find that r is always larger than 1. A rougher surface could lead to a higher roughness ratio and the apparent contact angle could also increase, which further enhance its hydrophobicity. Similarly, the rougher surface could enhance the hydrophilicity of the sample under the Wenzel state, which explains the lower WCA value on rougher surface after the plasma cleaning.

Comparing the storage conditions between ambient air and vacuum (the parallel experiments in vacuum, as indicated in Fig.2), the main difference could be the levels of the hydrocarbon groups. The comparative results indicate that the hydrocarbon groups in ambient atmosphere play vital roles in determining the wettability transition from hydrophilic to hydrophobic. It also verifies the function of plasma cleaning which mainly focuses on the cleaning function (to the as-prepared state), but not introducing a layer for the hydrophilicity.

The extent of WCA recovery varies significantly with SS samples, ED and ELD coatings. It is widely believed that changes in surface morphology and variations in surface chemistry could result in the wettability change. The main reason may stem

from the two aspects:

The first factor is surface composition. The adsorbed gaseous groups on the sample surfaces could be responsible for the variations of the wettability. The XPS analysis on ED and ELD samples show that the surface hydrocarbon groups and oxygen groups play vital roles in the surface wettability.

For carbon contents, the decrease of hydrocarbon groups in ED samples before and after plasma cleaning (Fig.5 (a) from 87.1% to 72.1%) is consistent with the sharp WCA decrease, which indicates the removal or decrease of the hydrocarbon coverage. The plasma cleaning treatment could drive away the physisorption of the airborne hydrocarbons. Furthermore, the decrease of non-polar groups on the surface would take place, leading to the increase of surface energy [42]. The recovery of WCA on ELD sample during the storage could be explained by the increased carbon contents (indicated in Fig.6(a) and Fig.6(b), from 74.0% to 81.7%), the reabsorbed hydrocarbon groups (mainly including C=C and C-C/C-H) would act as the hydrophobic defects on the sample surfaces [43]. There would be van der Waals bonding existing between the surfaces, which could increase the stability of the sample surface. Hence, the adsorption of hydrocarbon species could occur. The partial adsorption of the hydrocarbon groups onto the sample surface would be ongoing during the whole storage. Due to the coverage and spread of airborne hydrocarbon groups onto the surface, it finally leads to a hydrophilic-hydrophobic transition.

From the XPS results, the change of carbon content on the sample surfaces cannot completely explain the phenomenon of spontaneous wettability transition. The

oxygen groups could be another important factor, the variation in oxygen contents also contributes to the wettability change. First, the plasma cleaning of the ED sample (Fig.5(a) to Fig.5(b)) leads to the increase of lattice oxygen (O-metal, from 21.9% to 36.6%), which could promote the formation of hydrogen bonds with the interfacial water [44]. There would also be more hydrophilic groups (e.g. hydroxyls) involved onto the surface, causing the increase of surface free energy. It is reported that the WCA recovery could be attributed to the vibrational overtone transitions of hydroxyl groups [45]. Under such an environment, the O-metal groups are more likely to be adsorbed onto the hydrophilic surface and react with the moisture, which further affects the bonding between the water molecules. This could result in the water dissociation, and suppresses the formation of water clusters and creates hydrophilic surface sites [46, 47].

After long-time exposure to ambient air, the ELD samples exhibit obvious decrease in lattice oxygen groups (as shown in Fig.6), which indicates that the surface adsorption undergoes a continuous relaxation. The desorption of lattice oxygen from the sample surface and the readsorption of hydrocarbon groups would work in conjunction with the incident photon energy to release oxygen from the sample lattices [48]. Here, the surface adsorption of oxygen gaseous species (including hydroxyls and carbonates) could also contribute to the increase of non-lattice oxygen on the surface [6]. The formerly adsorbed oxygen molecules would dissociate at the position of oxygen vacancy during the storage. Therefore, the surface would spontaneously recover back to its former hydrophobic state during the storage [49].

The second factor is the surface roughness (surface topography): the diversity in surface roughness leads to the diverse WCA recovery process. It is assumed that the changing rate of WCA is depended on the available surface area which will be covered by the airborne hydrocarbons. Some calculations using the WCA variation results of different samples have been conducted to aid the understanding of WCA recoveries.

The hydrocarbon adsorption is proportional to the available surface area. It is speculated that the measured WCA shows a positive correlation with the available surface per unit area coated by the airborne hydrocarbon.

$$\frac{dW}{dt} = WCA\_inf - WCA \quad (2)$$

where *WCA_inf* is the value of WCA after infinite recovery time, corresponding to the stabilised WCA value. To solve this differential equation Eq (2), a boundary condition (t=0, WCA=WCA_0) is applied. WCA_0 is the value of WCA immediately after plasma cleaning. Then a sort of solution of the significant WCA recovery with a time constant (τ) could be obtained. Here, τ represents the characteristic timescale of the process, which mainly depended on the micro-scale convolution or roughness of the sample surface.

To further interpret the influencing factors of WCA recovery process, an exponential model is applied to fit the WCA recovery processes on different samples based on the former hypothesis. An analysis of the time constants with respect to the measured surface roughness is also attached in Tab.2. A model for the exponential WCA recovery based on the empirical evidence has been proposed as equation (3):

$$WCA(t) = WCA\_0 + (WCA\_inf - WCA\_0)(1 - exp(-t/\tau)) \quad (3)$$

Where *WCA_0*, *WCA_inf*, τ are the fitting parameters, *WCA_0* is the value of WCA immediately after plasma cleaning, *WCA_inf* is the value of WCA after infinite recovery time, τ is the time constant associated with the recovery process which is specified for certain samples.

The related data sets of the studied samples have then been fitted into the model with the three parameters using excel solver software. The detailed results are shown in Fig.7. The fitted equations are also presented in the figure for reference, with the starting point of just after the plasma cleaning. The constants and the surface roughness of the samples are provided in Tab.2.

Fig.7 shows the fitting results of WCA change of the different samples, the scattered points are the experimental data while the curves are the fitting results. The fitted equations of the WCA changing curves have also been provided. It is obvious to see that the applied model Eq (3) works fairly fine with the experimental data, indicating a higher fitting match degree [50]. The corresponding equations and the three fitting parameters of each fitted curved are also given in Fig.7. Tab.2 presents the values of the involved parameters. From Fig.7(a) to Fig.7(c), the three samples have the same chemical composition, while the only difference lies in the surface roughness. The SS-rough possesses the highest WCA and suffers the biggest descend range. While for the SS-AR and SS-polish, the WCA decrease is smaller. SS-rough takes much more time than the other two samples to recover to their previous WCA levels. The phenomenon is also consistent with the analysis in ED and ELD coatings

in Fig.7(d) and Fig.7(e).

After the time constant (τ) is confirmed, the relationship between the time constant and the sample surface roughness could also be established. As shown in Fig.8, an attempt has been made to plot the surface roughness as X axis versus τ as Y axis. A linear fitting has also been established from the data set.

From Fig.8, it is observed that higher surface roughness contributes to larger time constant (τ). As discussed, higher surface roughness contributes to larger WCA recovery speed. So it is proposed that τ represents the characteristic timescale of the whole WCA recovery process, which mainly depends on how convoluted or rough the surface is. With more specific surface area, there will be more airborne hydrocarbon adsorbed onto the surface. This could accelerate the surface adsorption of airborne hydrocarbon species in ambient atmosphere. With the proposed model on WCA recovery process, it also offers good theoretical justification to relevant time-dependent wettability study.

On the other hand, the rougher surface also increases the difficulty to complete the WCA recovery since the WCA drop is also much larger after the plasma cleaning treatment, leading to a longer recovery duration. The surface would take more time to finish the process of replacing, inserting into, and/or covering the formerly adsorbed hydrophilic groups, such as -OH, COOH/C=O, lattice oxygen (O-metal) groups.

4. Conclusion

This work describes the understandings of spontaneous wettability transition

behaviour on metallic surfaces with different surface roughness. It was found that the surfaces of the SS samples and Ni-Cu-P coating samples exhibited similar wettability transitions with the assistance of plasma cleaning and ambient air storage. The variations of surface adsorption and lattice oxygen groups were responsible for the wettability transition. A model for exponential WCA recovery based on the empirical evidences of current study has also been proposed. The surface roughness could affect the specific surface area and the characteristic timescale of the whole WCA recovery process. Larger available surface area contributes to higher rate of hydrocarbon adsorption. The phenomenon could be considered in practical operation, while the importance of controlling hydrocarbon adsorption for material wetting behaviours needs to be highlighted. The acceleration and control of the time-dependent wettability or adsorption behaviours could also be a critical consideration in future investigation.

Acknowledgments: J.W. and M.J.W. contributed equally to this work. The work is supported by a joint Ph.D. studentship between China Scholarship Council (CSC) and The University of Nottingham. The authors acknowledge the use of facilities at Nanoscale and Microscale Research Centre of the University of Nottingham. This research was supported in part by the Scientific Research Foundation of Nanjing Institute of Technology (YKJ202106) and University of Nottingham Propulsion Futures Beacon for funding under Grant PF016 and PF020.

References:

[1] Y.C. Leem, J.S. Park, J.H. Kim, N. Myoung, S.Y. Yim, S. Jeong, W. Lim, S.T. Kim, S.J. Park, Light‐Emitting Diodes with Hierarchical and Multifunctional Surface Structures for High Light Extraction and an Antifouling Effect, Small 12(2) (2016) 161-168.

[2] Y. Shao, J. Zhao, Y. Fan, Z. Wan, L. Lu, Z. Zhang, W. Ming, L. Ren, Shape memory superhydrophobic surface with switchable transition between “Lotus Effect” to “Rose Petal Effect”, Chem Eng J 382 (2020) 122989.

[3] J. Kuang, Z. Ba, Z. Li, Z. Wang, J. Qiu, The study on corrosion resistance of superhydrophobic coatings on magnesium, Appl Surf Sci 501 (2020) 144137.

[4] W. Yao, O.L. Li, Y.-J. Kang, M.-Y. Jeong, Y.-R. Cho, Impact of pillar configuration on the amphiphobicity of micro-patterned polymer surface, Vacuum 156 (2018) 115-122.

[5] V.A. Dhumale, P.V. Shah, I. Mulla, R. Sharma, Switching of hydrophilic to ultra hydrophilic properties of flower-like gold nanostructures, Appl Surf Sci 256(13) (2010) 4192-4195.

[6] S. Lei, F. Wang, W. Li, G. Qiao, Reversible wettability between superhydrophobicity and superhydrophilicity of Ag surface, Sci China Mater 59(5) (2016) 348-354.

[7] P. Liu, L. Cao, W. Zhao, Y. Xia, W. Huang, Z. Li, Insights into the superhydrophobicity of metallic surfaces prepared by electrodeposition involving spontaneous adsorption of airborne hydrocarbons, Appl Surf Sci 324 (2015) 576-583.

[8] D. Zhu, Z. Shi, X. Tan, J. Zhang, S. Zhang, X. Zhang, Accelerated wetting transition from hydrophilic to hydrophobic of sputtered Cu films with micro-scale patterns, Appl Surf Sci 527 (2020) 146741.

[9] B. Wang, X. Wang, H. Zheng, Y. Lam, Femtosecond laser-induced surface wettability modification of polystyrene surface, Sci China Phys, Mech 59(12) (2016) 1-5.

[10] C. Florian, E. Skoulas, D. Puerto, A. Mimidis, E. Stratakis, J. Solis, J. Siegel, Controlling the wettability of steel surfaces processed with femtosecond laser pulses, ACS appl Mater & Inter 10(42) (2018) 36564-36571.

[11] D. Kim, J.G. Kim, C.N. Chu, Aging effect on the wettability of stainless steel, Mater Lett 170 (2016) 18-20.

[12] W. Zhang, D. Zhang, W. Yan, W. Luo, C. Zhao, D. Liu, Optically Induced Rapid Wetting Transition on Zn-Polar and O-Polar Zinc Oxide, Langmuir 35(46) (2019) 14791-14796.

[13] L. Hu, X. Song, X. Shan, X. Zhao, F. Guo, P. Xiao, Visible light-activated self-recovery hydrophobic CeO_2/black TiO_2 coating prepared using air plasma spraying, ACS appl Mater & Inter 11(40) (2019) 37209-37215.

[14] M. Mortazavi, M. Nosonovsky, A model for diffusion-driven hydrophobic recovery in plasma treated polymers, Appl Surf Sci 258(18) (2012) 6876-6883.

[15] E. Occhiello, M. Morra, P. Cinquina, F. Garbassi, Hydrophobic recovery of oxygen-

plasma-treated polystyrene, Polymer 33(14) (1992) 3007-3015.
[16] S. Choudhury, S. Roy, G. Bhattacharya, S. Fishlock, S. Deshmukh, S. Bhowmick, J. McLaughlign, S.S. Roy, Potentiometric ion-selective sensors based on UV-ozone irradiated laser-induced graphene electrode, Electrochim Acta 387 (2021) 138341.
[17] T. Sönmez, M.F. Jadidi, K. Kazmanli, Ö. Birer, M. Ürgen, Role of different plasma gases on the surface chemistry and wettability of RF plasma treated stainless steel, Vacuum 129 (2016) 63-73.
[18] T. Demina, D. Zaytseva-Zotova, M. Yablokov, A. Gilman, T. Akopova, E. Markvicheva, A. Zelenetskii, DC discharge plasma modification of chitosan/gelatin/PLLA films: Surface properties, chemical structure and cell affinity, Surf Coat Tech 207 (2012) 508-516.
[19] S.-J. Hwang, M.-C. Tseng, J.-R. Shu, H.H. Yu, Surface modification of cyclic olefin copolymer substrate by oxygen plasma treatment, Surf Coat Tech 202(15) (2008) 3669-3674.
[20] J. Wang, J. Liu, N. Neate, M. Bai, F. Xu, T. Hussain, C. Scotchford, X. Hou, Investigation on time-dependent wetting behavior of Ni-Cu-P ternary coating, J Alloy Compd 765 (2018) 221-228.
[21] J. Wang, H. Memon, J. Liu, G. Yang, F. Xu, T. Hussain, C. Scotchford, X. Hou, Effect of surface adsorption on icing behaviour of metallic coating, Surf Coat Tech 380 (2019) 125068.
[22] A. Vladar, M. Postek, Electron beam-induced sample contamination in the SEM, Microsc Microanal 11(S02) (2005) 764-765
[23] G. Greczynski, L. Hultman, X-ray photoelectron spectroscopy: towards reliable binding energy referencing, Prog Mater Sci 107 (2020) 100591.
[24] E.F. Smith, J.D. Counsell, J. Bailey, J.S. Sharp, M.R. Alexander, A.G. Shard, D.J. Scurr, Sample rotation improves gas cluster sputter depth profiling of polymers, Surf Interface Anal 49(10) (2017) 953-959.
[25] G. Greczynski, D. Primetzhofer, L. Hultman, Reference binding energies of transition metal carbides by core-level x-ray photoelectron spectroscopy free from Ar^+ etching artefacts, Appl Surf Sci 436 (2018) 102-110.
[26] A. Modabberasl, P. Kameli, M. Ranjbar, H. Salamati, R. Ashiri, Fabrication of DLC thin films with improved diamond-like carbon character by the application of external magnetic field, Carbon 94 (2015) 485-493.
[27] G. Greczynski, L. Hultman, The same chemical state of carbon gives rise to two peaks in X-ray photoelectron spectroscopy, Sci Rep 11(1) (2021) 1-5.
[28] G. Greczynski, L. Hultman, In-situ observation of self-cleansing phenomena during ultra-high vacuum anneal of transition metal nitride thin films: Prospects for non-destructive photoelectron spectroscopy, Appl Phys Lett 109(21) (2016) 211602.
[29] G. Greczynski, L. Hultman, Compromising science by ignorant instrument calibration - Need to revisit half a century of published XPS data, Angew Chem Int Ed 59 (2020) 5002.
[30] G. Greczynski, L. Hultman, C 1s peak of adventitious carbon aligns to the vacuum level:

dire consequences for material's bonding assignment by photoelectron spectroscopy, ChemPhysChem 18(12) (2017) 1507.
[31] G. Greczynski, L. Hultman, Reliable determination of chemical state in x-ray photoelectron spectroscopy based on sample-work-function referencing to adventitious carbon: resolving the myth of apparent constant binding energy of the C 1s peak, Appl Surf Sci 451 (2018) 99-103.
[31] G. Greczynski, S. Mráz, L. Hultman, J. Schneider, Unintentional carbide formation evidenced during high-vacuum magnetron sputtering of transition metal nitride thin films, Appl Surf Sci 385 (2016) 356-359.
[32] G. Greczynski, L. Hultman, Reliable determination of chemical state in x-ray photoelectron spectroscopy based on sample-work-function referencing to adventitious carbon: resolving the myth of apparent constant binding energy of the C 1s peak, Appl Surf Sci 451 (2018) 99-103.
[33] W. Sachtler, G. Dorgelo, The surface of copper-nickel alloy films: I. Work function and phase composition, J Catal 4(6) (1965) 654-664.
[34] C.-H. Chen, B.-H. Chen, L. Hong, Role of Cu^{2+} as an Additive in an Electroless Nickel-Phosphorus Plating System: A Stabilizer or a Codeposit?, Chem Mater 18(13) (2006) 2959-2968.
[35] Y. Cheng, Y. Zheng, X. Huang, K. Zhong, Z. Chen, Z. Huang, Magnetism and work function of Ni-Cu alloys as metal gates, Rare Metals 31(2) (2012) 130-134.
[36] G. Xu, Q. Wu, Z. Chen, Z. Huang, Y.P. Feng, Effects of surface alloying and orientation on work function of MoTa metal gate, J Appl Phys 106(4) (2009) 043708.
[37] S. Lin, D. Xie, Y. Tang, Y. Wang, F. Jing, N. Huang, Y. Leng, Effect of nitrogen flow on the properties of carbon nitride films deposited by electron cyclotron resonance plasma-enhanced chemical vapor deposition, Vacuum 189 (2021) 110223.
[38] A.V. Naumkin, A.K. Vass, S.W. Gaarenstroom, C.J. Powell. US Department of Commerce, NIST Data Resources for X-Ray Photoelectron Spectroscopy, Surf Interface Anal (2000).
[39] S. Khan, G. Azimi, B. Yildiz, K.K. Varanasi, Role of surface oxygen-to-metal ratio on the wettability of rare-earth oxides, Appl Phys Lett 106(6) (2015) 061601.
[40] H. Yuan, B.T. Kusema, Z. Yan, S. Streiff, F. Shi, Highly selective synthesis of 2, 5-bis (aminomethyl) furan via catalytic amination of 5-(hydroxymethyl) furfural with NH_3 over a bifunctional catalyst, RSC Adv 9(66) (2019) 38877-38881.
[41] L. Hu, X. Song, X. Shan, X. Zhao, P. Xiao, Visible Light Activated Self-Recovery Hydrophobic CeO_2 /Black TiO_2 Coating Prepared Using Air Plasma Spraying, ACS appl Mater & Inter 11(40) (2019) 37209-37215.
[42] R. Ashiri, A Mechanistic Study of Nanoscale Structure Development, Phase Transition, Morphology Evolution, and Growth of Ultrathin Barium Titanate Nanostructured Films, Metall Mater Trans A 45(9) (2014) 4138-4154.

[43] R. Raj, R. Enright, Y. Zhu, S. Adera, A. Wang, Unified Model for Contact Angle Hysteresis on Heterogeneous and Superhydrophobic Surfaces, Langmuir 28(45) (2012) 15777-15788.
[44] J. Fan, X. Wu, Y. Lei, W. Duan, The SMSI between supported platinum and CeO_2-ZrO_2-La_2O_3 mixed oxides in oxidative atmosphere, Catal Today 126(3-4) (2007) 303-312.
[45] J.A. Curcio, C.C. Petty, The Near Infrared Absorption Spectrum of Liquid Water, Journal of the Optical Society of America 41(5) (1951) 302-304.
[46] D.J. Preston, N. Miljkovic, J. Sack, R. Enright, J. Queeney, E.N. Wang, Effect of hydrocarbon adsorption on the wettability of rare earth oxide ceramics, Appl Phys Lett 105(1) (2014) 011601.
[47] D. Zhang, W. Yan, W. Luo, W. Zhang, C. Zhao, D. Liu, Promoted reversible wettability transition by plasmonic effects at Ag/TiO_2 heterointerface, Appl Phys Lett 114(4) (2019) 041602.
[48] Y. Shapira, and, M. S., Cox, and, David, Lichtman, Chemisorption, photodesorption and conductivity measurements on ZnO surfaces, Surf Sci 54(1) (1976) 43-59.
[49] D. Zhao, R. Jia, N. Gao, W. Yan, L. Zhang, X. Li, D. Liu, Near-infrared promoted wettability recovery of superhydrophilic ZnO, J Phys Chem C 121(23) (2017) 12745-12749.
[50] T.J. Zielinski, R.D. Allendoerfer, Least squares fitting of non-linear data in the undergraduate laboratory, J Chem Educ 74(8) (1997) 1001.

List of Figure Captions

List of Table Captions

Table.1

	Detailed conditions	Hydrocarbon in all (at%)	Lattice Oxygen (at%)	WCA/°
ED sample	Before Plasma	87.1	21.9	140.8±4.6°
	Just after Plasma	72.1	36.6	7.8±0.2°
ELD sample	Just after Plasma	74.0	50.6	17.7±0.9°
	Long ambient air exposure	81.7	15.1	106.1±4.2°

Table.2

Samples	Time constant (τ)	Surface roughness/μm
SS-polish	3.55	0.06±0.01
SS-AR	4.87	0.2±0.01
SS-rough	38.28	1.0±0.03
ELD	6.68	0.5±0.02
ED	70.21	3.9±0.10

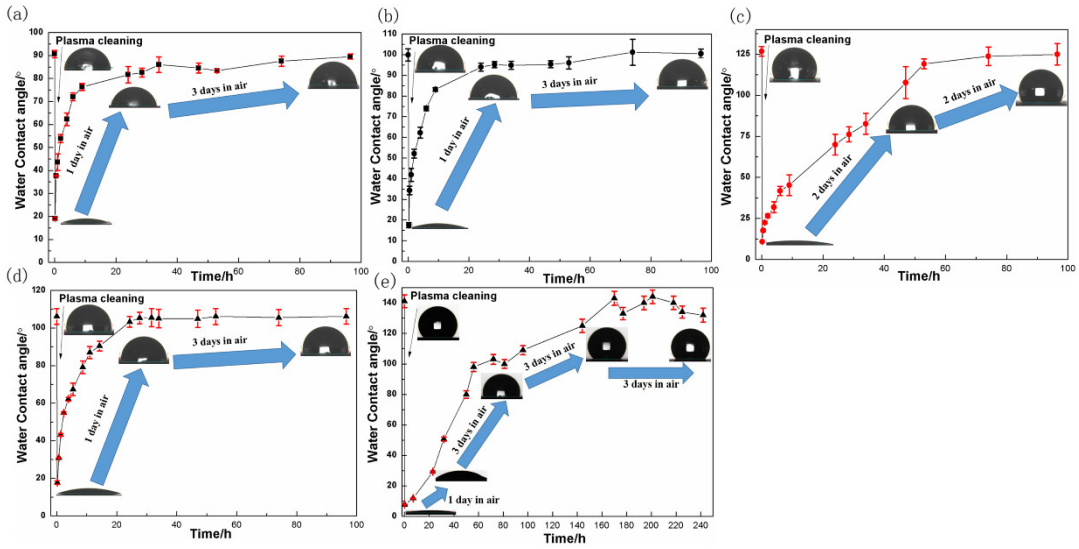

Figure 1 Changes of WCAs of SS samples and Ni-Cu-P coatings with plasm cleaning and aging in ambient air (a) SS-polish (b) SS-AR (c) SS-rough (d) ELD sample (e) ED sample

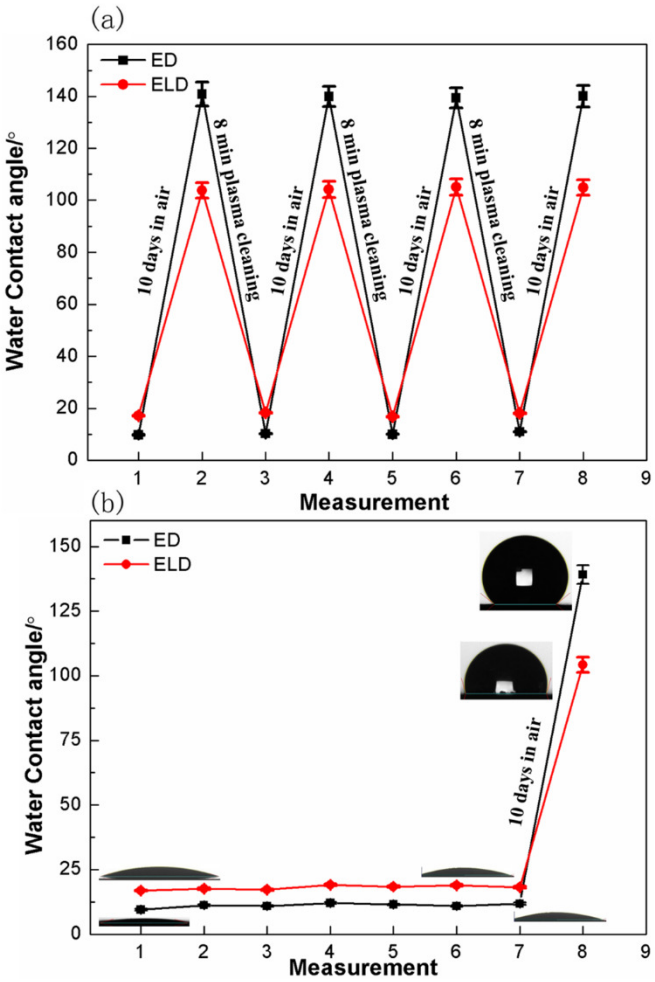

Figure 2 (a) Reversible wettability of ED and ELD samples during cycles of ambient air storage and plasma cleaning (b) Variation of WCAs of ED and ELD samples in vacuum storage

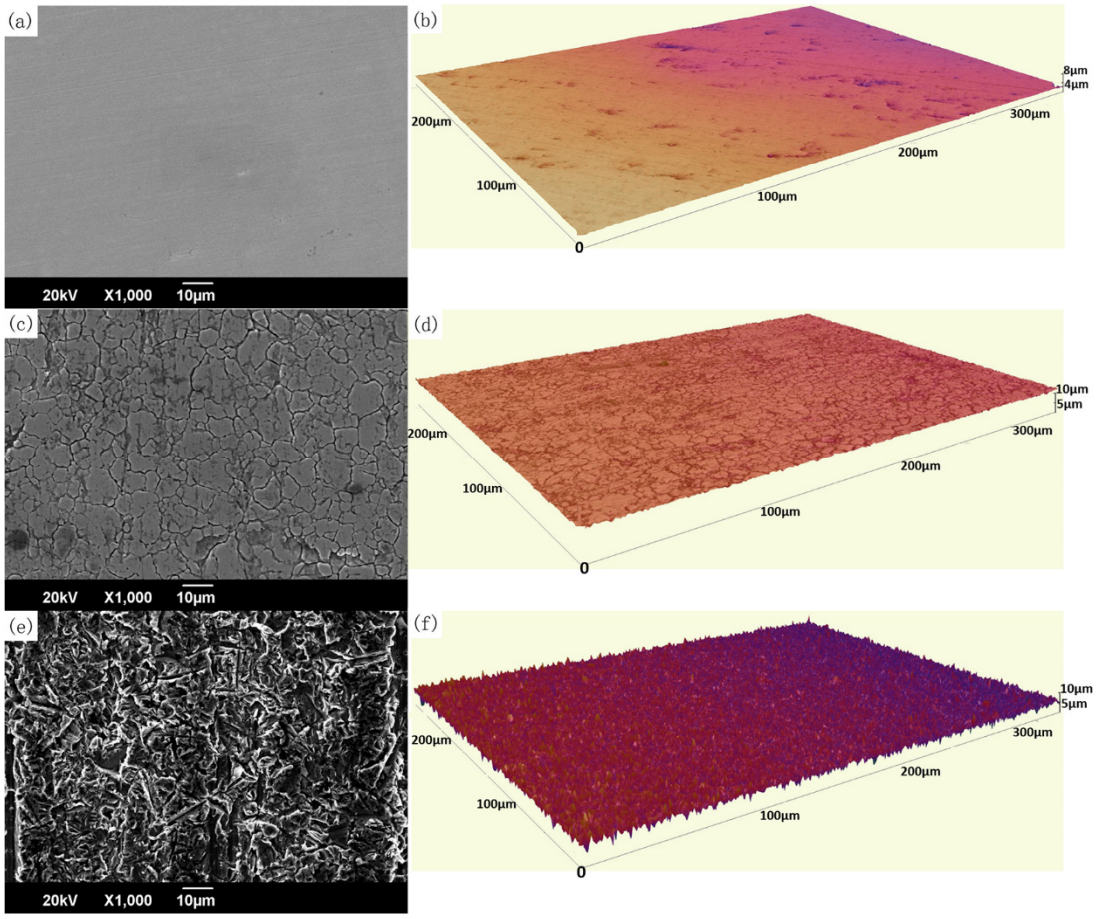

Figure 3 SEM images of surface morphologies (a) SS-polish (c) SS-AR (e) SS-rough; and 3D topography images of (b) SS-polish (d) SS-AR (f) SS-rough

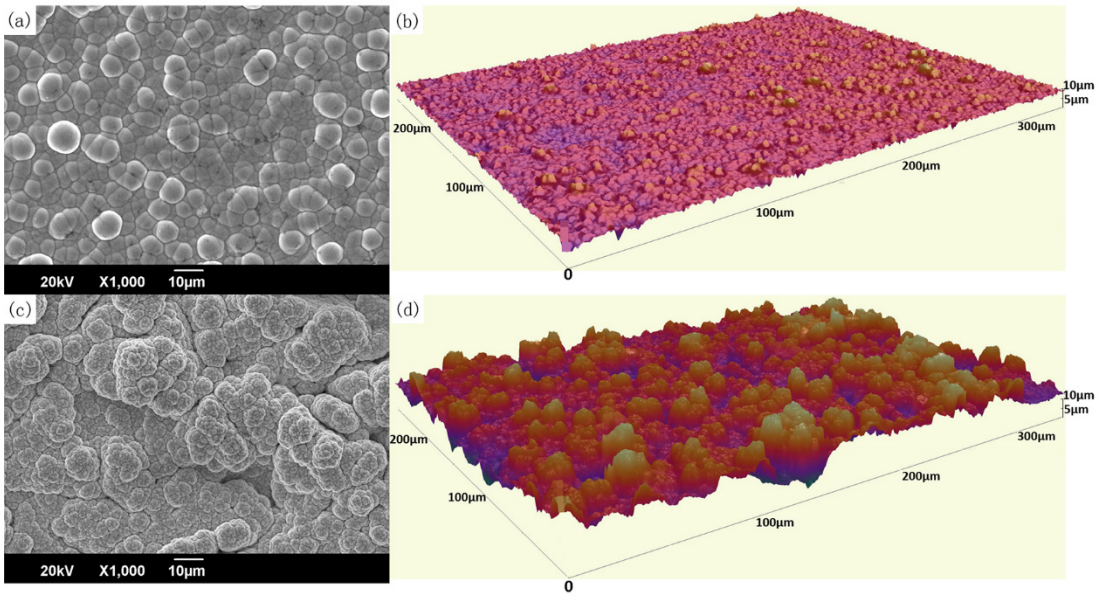

Figure 4 SEM images of surface morphologies (a) ELD (c) ED, and 3D topography images of (b) ELD (d) ED

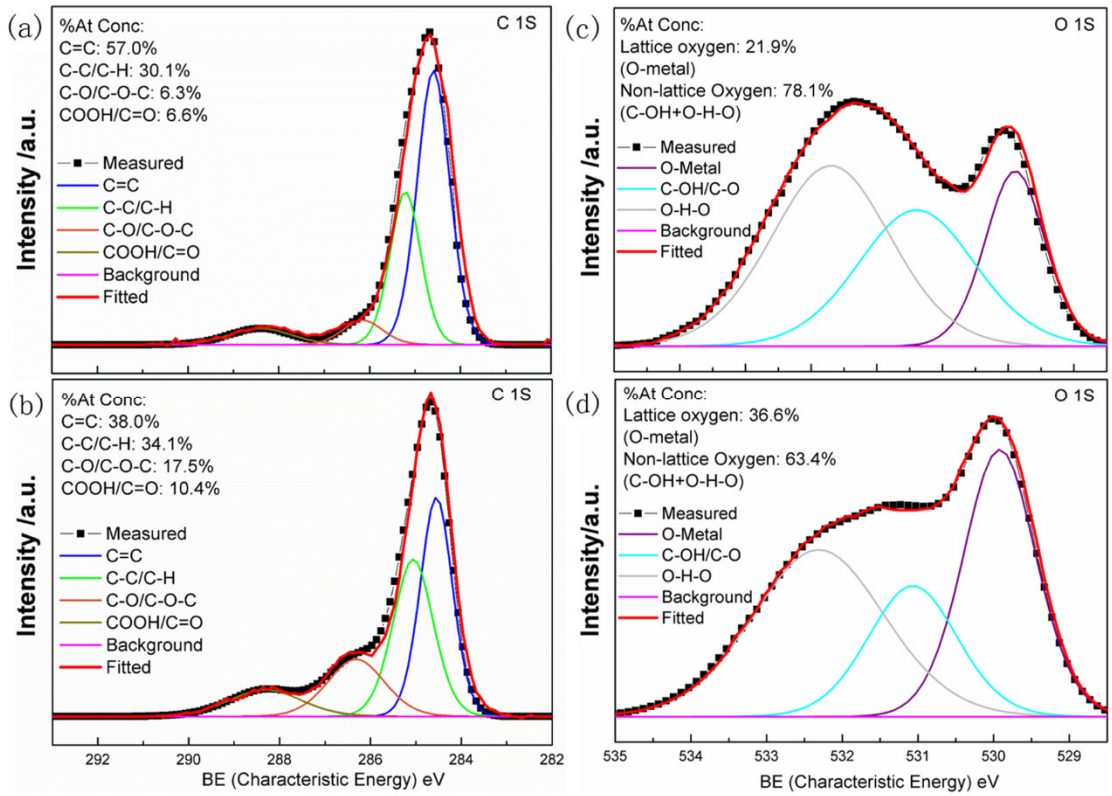

Figure 5 (a) and (b) C 1s XPS spectra of the ED coating versus plasma cleaning (a) Before plasma (b) Just after plasma; (c) and (d) O 1s XPS spectra of the ED coating versus plasma cleaning (c) Before plasma (d) Just after plasma

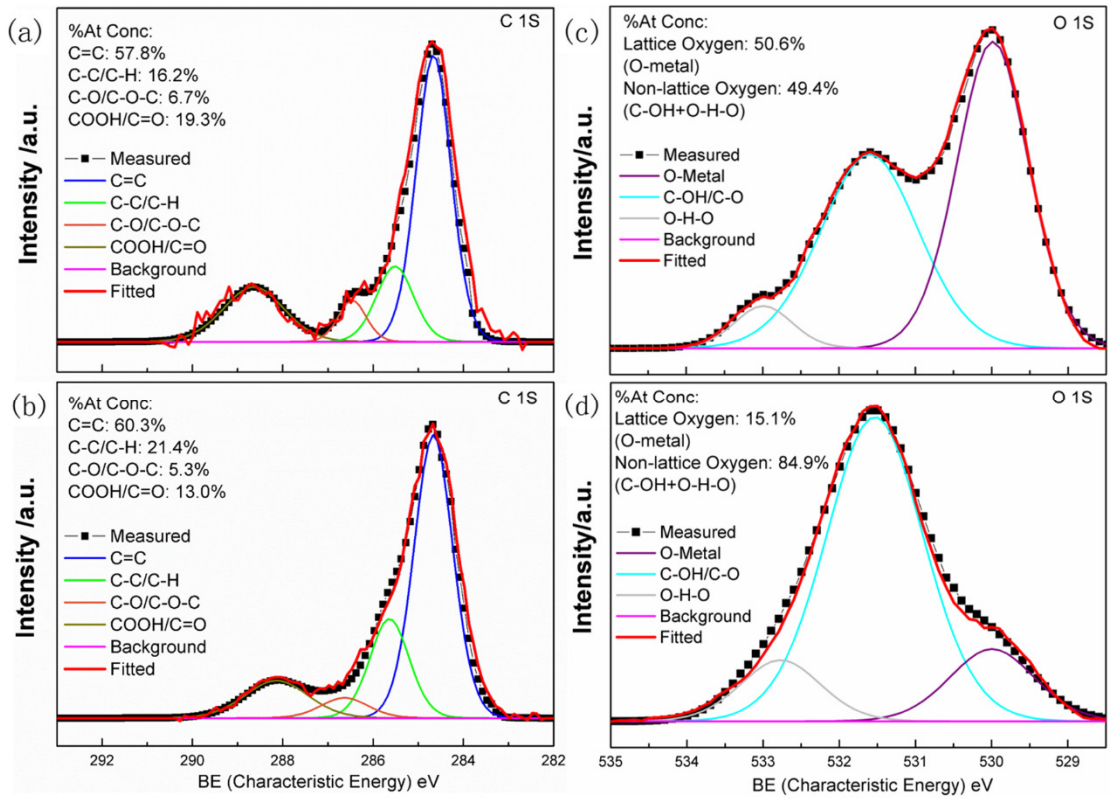

Figure 6 (a) and (b) C 1s XPS spectra of the ELD coating (a) Just after plasma cleaning (b) After long storage in ambient air; (c) and (d) O 1s XPS spectra of the ELD coating (c) Just after plasma cleaning (d) After long storage in ambient air

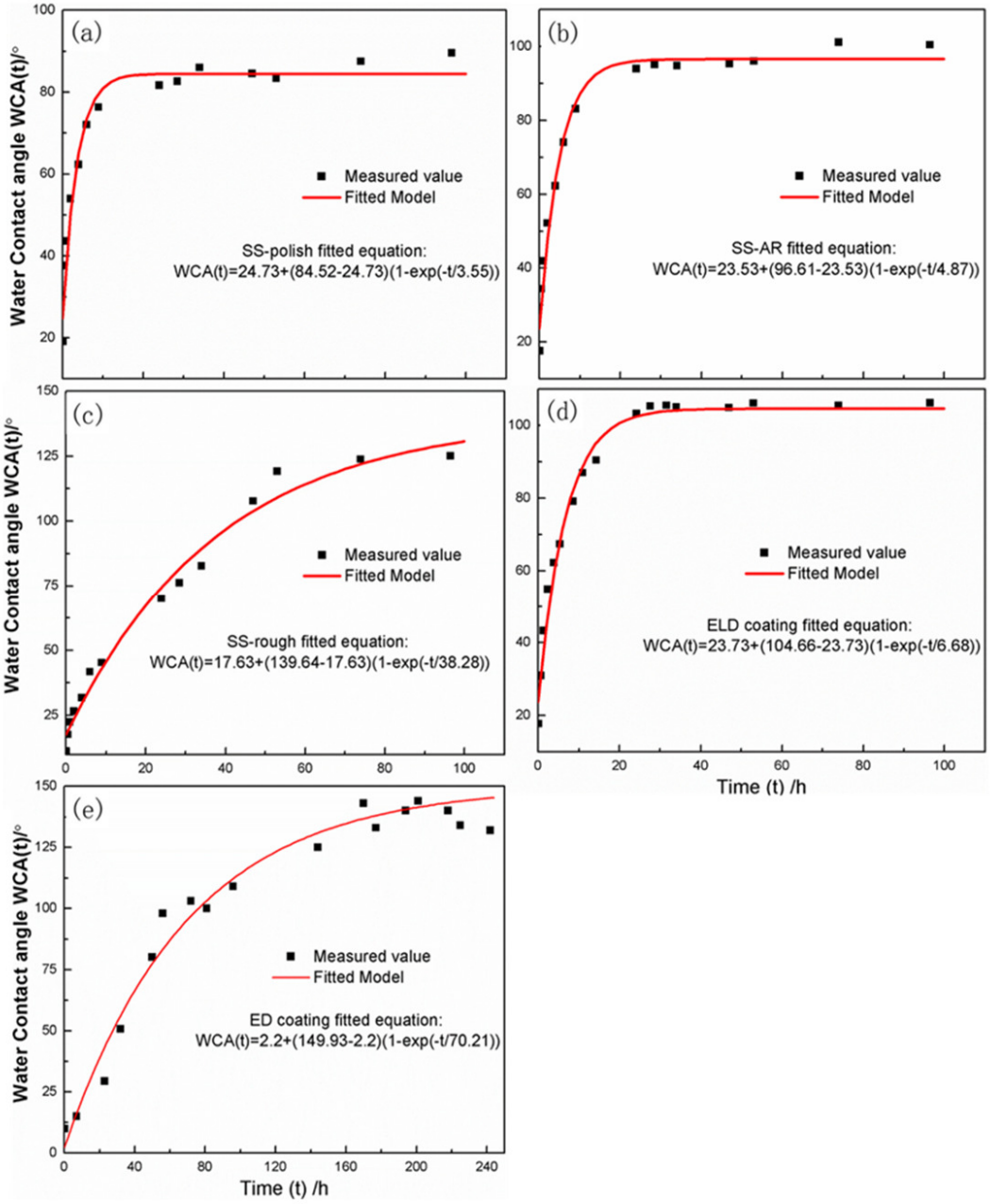

Figure 7 Exponential fitted models of the WCA change versus time on different samples including (a) SS-polish, (b) SS-AR, (c) SS-rough, (d) ELD coating and (e) ED coating

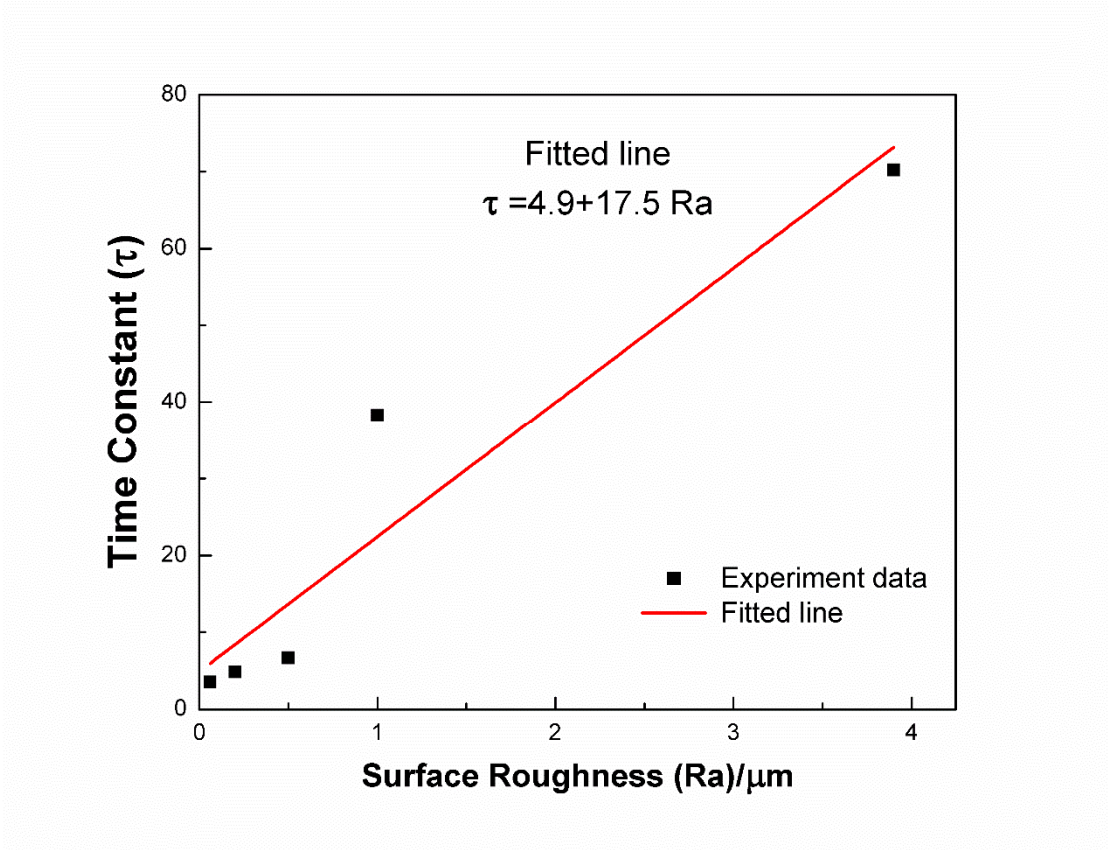

Figure 8 Relationship and fitted line of time constant (τ) and surface roughness during WCA recovery process on different samples